QUANTIFICATION OF DCE-MRI: A VALIDATION OF THREE TECHNIQUES WITH 3D-HISTOLOGY

Karin Bol[abc], Joost C. Haeck[abc], Lejla Alic[ab], Wiro J. Niessen [abd]
Marion de Jong[bc], Monique Bernsen[bc], Jifke F. Veenland[ab]

[a]BIGR – Biomedical Imaging Group Rotterdam, [b]Department of Radiology and [c]Nuclear Medicine, Erasmus MC, Rotterdam, P.O. Box 2040, 3000 CA Rotterdam, The Netherlands;
[d]Faculty of Applied Sciences, Delft University of Technology, Delft, The Netherlands

ABSTRACT

Three different DCE-MRI quantification methods: model-free-based, compartment-model-based and principal component analysis, are compared by evaluating parameter maps for histological defined volumes of vital and non-vital tumor tissue. To obtain an accurate spatial correspondence between histology and DCE-MRI, a two-step registration process was used involving dense histological sampling, a reference plane and an intermediate ex vivo MRI. Results show that the model-free parameter wash-out and the second principal component score can adequately separate vital from non-vital tumor tissue, with an accuracy of respectively 99.2% and 99.7%. The other model-free parameters and the compartment-model-based Ktrans show some overlap in values between vital and non-vital tissue. The first, third and fourth pc-score have limited discriminative power.

Index Terms— DCE-MRI, histology, Principal Component Analysis, standard Tofts model, model-free analysis

1. INTRODUCTION

In oncology, Dynamic Contrast-Enhanced Magnetic Resonance Imaging (DCE-MRI) is increasingly used as a tool to detect tumors or metastases, to monitor tumor growth, and to assess and predict the response to anti-tumor treatment. Although many different analysis methods have been proposed to quantify tumor characteristics from DCE-MRI data, a standard analysis method has not yet been adopted.

In DCE-MRI the signal intensity over time is acquired following contrast injection. Both model-free and compartment-model-based methods can be employed to analyze the signal-intensity-time curves (SI-curves) obtained from the DCE images[1]. Model-free parameters are derived directly from the SI-curves, for example the area under the curve (AUC), wash-in and wash-out rate of the contrast agent and maximal enhancement (Smax). These parameters are straightforward and easy to implement, however, they are not necessarily correlated with underlying physiological tumor characteristics. Furthermore, it is difficult to compare measurements from scans acquired at different times or from different scanners, owing to the lack of an absolute intensity scale in MRI.

Compartment-model-based methods use pharmaco-kinetic modeling to quantify the concentration time curve. These models assume that the tissue is divided into several compartments limiting the exchange of contrast agent. The number of compartments can vary per model[1,3]. For the computation of the kinetic parameters, additional information is required, such as a T1-map for the contrast-concentration computation and an Arterial Input Function (AIF). Multiple methods for acquiring and fitting a T1-map or AIF exist[1,2,9], influencing the resulting parameter value. Moreover, fitting of the compartment model to the curve is computationally more expensive than model free methods,.

Recently principal component analysis (PCA) has been proposed as an alternative[3,5,6] to the more conventional model-free and compartment-model-based methods. Bruwer et.al.[3] states that PCA offers an improvement over the other two methods because the responses of all voxels are included simultaneously rather than estimating parameters separately for each voxel. Also in PCA the whole time-trajectory is considered instead of certain aspects of that trajectory (e.g. wash-in). As a consequence the resulting parametric maps (pc-scores) will be more robust against image noise. Furthermore, PCA does not require an AIF and fits the actual structure in the data rather than the assumed structure arising from the chosen compartment model.

For the validation of the different DCE-MRI based parameters, histology is still the gold-standard[1]. Matching 3D-histology to MRI is hampered by changes in morphology due to shrinkage and orientation once specimens are dissected and placed in formalin fixative. To achieve accurate co-localization between 3D-histology and MRI, we developed a multi-step registration framework involving dense histological sampling, a reference plane and an intermediate ex vivo MRI[7]. Using this registration framework, the correspondence of DCE-MRI derived parameters with vital and non-vital tumor tissue can be investigated[8]. In this study we compare the discriminative

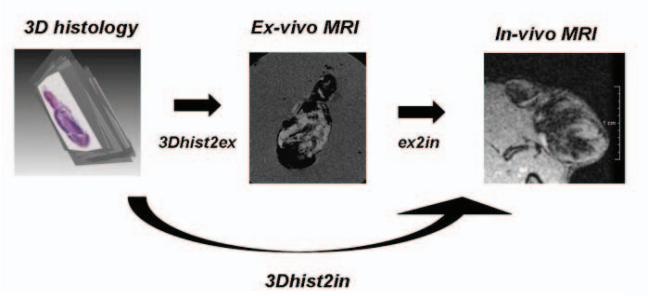


Figure 1; Registration Scheme of Alic et. al.[7]

power of parameters derived from three different DCE-MRI quantification methods, namely, model-free-based, compartment-model-based, and PCA, between vital and non-vital tumor tissue.

2. MATERIALS AND METHODS

2.1. Animal and tumor model

For this study, male Lewis rats (Harlan_CPB, Austerlitz, The Netherlands), weighing approximately 300 grams, were used with approval of the Committee for Animal Research of the Erasmus MC, Rotterdam, The Netherlands. Pancreatic tumor cells (CA20948 tumor) were inoculated subcutaneously in the right hind limb. The tumors were imaged when they reached a diameter of 1.5-2 cm. The animals were anesthetised before imaging using Isoflurane (Nicholas Pyramal Limited, London, UK). After completing the examinations the animals were sacrificed and the tumors were dissected and processed for further analysis.

2.2. DCE-MRI imaging protocol

A clinical 3 Tesla MRI scanner (Signa Excite, GE Healthcare, USA) was used for imaging. DCE images were obtained using TRICKS (Time Resolved Imaging of Contrast Kinetics) in order to achieve a high temporal resolution: 165 images were made with a temporal resolution of 4.2 s. These images were acquired in 5 sequential acquisitions with 4 intervals in between, spanning a total time frame of 30 minutes. T1-weighted MR images were used for calibration of the DCE data and in vivo as well as ex vivo susceptibility-weighted images (SWI) were used for registration purposes. In vivo MRI settings were: T1-weighted: TR/TE=20/4 ms, flip angles of 3, 5, 10, 15, 20, 35 and 50º and a XYZ resolution of 0.2x0.2x0.7; SWI: TR/TE=24.4/12.0 ms, flip angel of 10º and a XYZ resolution of 0.098x0.098x0.20; TRICKS: TR/TE=5.44/1.46 ms, flip angle of 10º, XYZ resolution of 0.2x0.2x0.7. Ex vivo SWI settings were: TR/TE=23.5/8.9 ms, flip angel of 10º and a XYZ resolution of 0.098x0.098x0.40.

2.3. Data acquisition and image registration

A previously developed framework for data acquisition and image registration was used[8]. In short: after in vivo MR, the tumor was dissected and dyed to track its orientation with respect to the in vivo situation. After a week in formalin a small piece of the tumor, perpendicular to the longitudinal axis of that tumor, was cut off defining a plane of reference for ex vivo MRI and creating a cutting plane for histology. After ex vivo MR imaging, the tumor was embedded in paraffin and sections of 4 µm at 80 µm intervals were cut using a microtome. The sections were fixed on a glass slide, stained with haematoxylin and eosin (H&E) and digitized using the NanoZoomer (C9600. Hamamatsu, Japan). The digitized histology slices were then stacked into a 3D volume using a rigid registration scheme. To match the 3D histology volume to the in vivo DCE-MR images, the two-step registration scheme of Alic et.al[7] was used (figure 1). First the 3D histology was registered to the ex vivo MRI and then the ex vivo MRI was registered to the in vivo MRI. Transformation parameters resulting from the second step were used to transform the 3D histology to in vivo MRI. All registrations were performed with Elastix (http://elastix.isi.uu.nl/), using non-rigid B-splines with a mutual information metric and a 4 level Gaussian pyramid.

2.4. DCE-MRI quantification

2.4.1. Model-free parameters

From the SI-curve model-free parameters (i) maximum enhancement (Smax), (ii) area under the curve for the first 60 seconds (AUC60), (iii) wash-in rate and (iv) wash-out rate were calculated for voxels in the tumor.

2.4.2. Compartment- model- based parameters

For voxels in the tumor the SI-curves were converted to contrast-concentration curves using a linearized T1-mapping method[9]. To obtain the AIF, voxels in an artery near the tumor were selected. The average enhancement curve for these voxels was fitted with a bi-exponential function to acquire parameters a_i and m_i. These were then inserted into the compartment-model-based standard Tofts equation[4]:

$$C(t) = DKtrans \sum_{i=1}^{2} \frac{a_i [\exp(-m_i t) - \exp(-k_{ep} t)]}{k_{ep} - m_i} \quad (1)$$

and this equation was fitted to the contrast-concentration curve. In this study only the parameter map of Ktrans resulting from this fit was used. From the standard Tofts fit we acquired an r-square map, and in all DCE parametric maps voxels where $r^2 \leq 0.5$ were excluded from further analysis.

2.4.3. Principal component analysis

Principal component analysis (PCA) was the third DCE-MRI analysis method we considered. From the 4D tumor

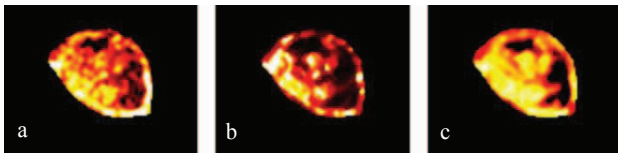


Figure 2; Examples of parametric maps, a) AUC60, b) Ktrans, c) second pc-score, yellow-white denotes high parameter values, whereas dark red-black denotes low parameter values.

enhancement data a 2D MxN matrix X can be constructed, with M being the number of voxels in the tumor and N the associated time-trajectory of image intensities[3]. PCA then estimates the correlation structure between the different enhancement curves of the whole dataset by transforming matrix X into a new orthogonal coordinate system[10]. The principal components P(N) determined in this way are linear combinations of the original variables of X. The first principal component displays the largest variation in the column-data of X, and the subsequent components are arranged in descending order of variation. Geometrically, the data matrix X can be plotted on N-dimensional space. If we consider dimension N, a straight line P(N) can be fitted to the points (M,N) in that dimension. If X(M,N) represent the coordinates of those points, the following relationship exists[10]:

$$X(M,N) = C(N) + T(M) * P(N) \qquad (2)$$

The so-called pc-scores T(M) are the orthogonal projections of points in dimension N on P(N). These scores can then serve as an alternative DCE-parameter, since for every P(N) the variance and thus the T(M) differs. To assess the influence of the contrast-concentration calculations, we performed also PCA on C(t) data (equation (1)).

2.5. Correspondence of DCE-MRI parameters with histology

To evaluate the correspondence of the different DCE parameters with histology, vital and non-vital regions were selected by drawing regions of interest (ROI's) on histology slices in the 3D volume. These regions were then transformed to the parametric maps, using the transformation parameters resulting from the image registration. For vital and non-vital parametric values scatterplots were made and a Fisher's linear disciminant leave-one-out analysis was performed to assess if the different DCE-parameters were able to distinguish between vital and non-vital tumor tissue.

3. RESULTS

Figure 2 shows representative parametric maps for each method, i.e., AUC60, Ktrans, and the second pc-score.

Figure 3 illustrates the correlation between DCE-parameters and vital and non-vital tumor tissue by showing scatterplots for three parameter pairs. The model-free

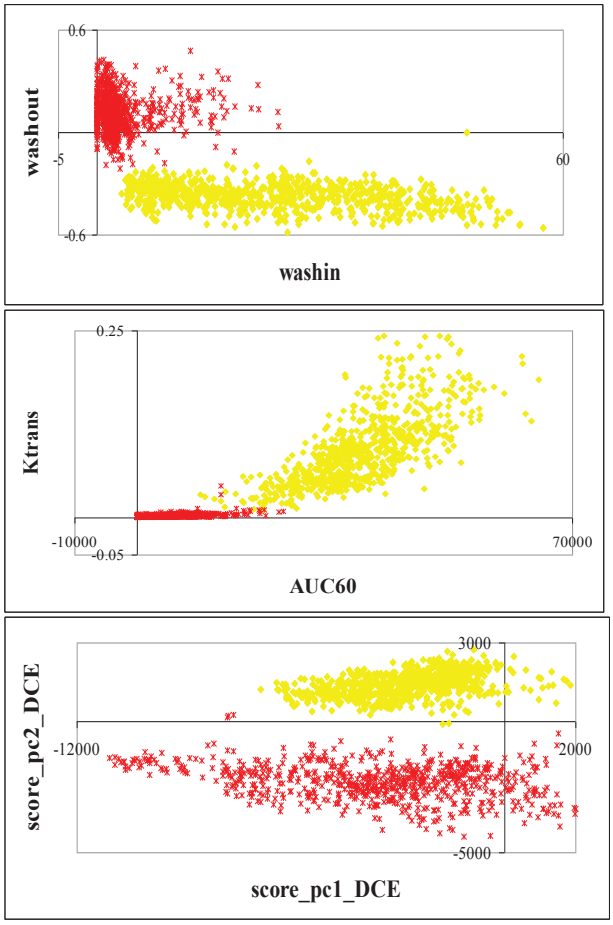


Figure 3; Scatterplots of vital (◆) versus non-vital (✳) tumor tissue for combinations of DCE parameters.

Table 1; Fisher's linear discriminant analysis: result of leave-one-out classification for vital voxels.

DCE parameter	Sensitivity (%)	Specificity (%)	Accuracy (%)
AUC60	96.4	99.6	98.0
Smax	98.4	95.0	96.7
wash-out	99.9	98.5	99.2
wash-in	70.3	95.9	83.0
Ktrans	81.2	100.0	90.5
1st pc-score Ct	59.9	76.4	68.1
2nd pc-score Ct	99.9	99.6	99.7
3rd pc-score Ct	58,1	63,3	60,7
4th pc-score Ct	60,7	63,9	62,3
1st pc-score DCE	60.3	51.9	56.2
2nd pc-score DCE	100.0	99.5	99.7
3rd pc-score DCE	68,7	34,0	51,5
4th pc-score DCE	60,9	54,9	57,9

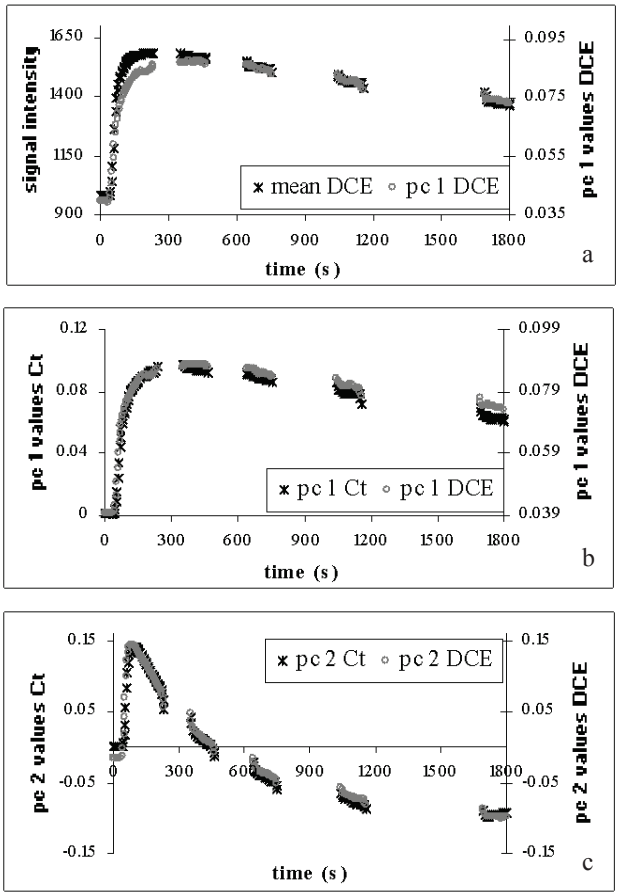


Figure 4; Comparing mean signal-enhancement DCE with the first principal component (a), mean contrast-concentration Ct with the first principle component (not shown) produced a similar graph; and comparing Ct with DCE for the first (b) and second (c) principal components; all voxels in the tumor were included.

parameter wash-out showed good separation between vital and non-vital tumor tissue. For AUC60, wash-in and Smax (not shown) there is some overlap in values between vital and non-vital tissue, just as for the compartment-model-based parameter Ktrans. Considering the PCA parameters, the second pc-score showed good separation, the first, third and fourth PC-score (not shown) were not able to separate vital and non-vital tissue. Using Fisher's linear discriminant analysis, the model-free parameter wash-out and the second pc-score show the highest sensitivity, specificity and accuracy in separating vital from non-vital tumor tissue (table 1).

Comparing the PCA computed from contrast-concentration data as opposed to the raw signal-intensity values, we found very similar results (table 1 and figure 4). As can be seen in figure 4 (b,c) the first two principal components for the raw signal-enhancement and contrast-concentration data are very similar. Furthermore, the shape of the first principal component resembled the mean enhancement for both data sets quite closely (figure 4a).

4. CONCLUSION AND FUTURE DIRECTIONS

This study demonstrates that DCE derived parametric maps can be validated using densely sampled 3D histology. For this tumor model three different quantification methods were compared. Wash-out and the second pc-score separated vital from non-vital tissue best. Ktrans, AUC60, wash-in and Smax showed some overlap between the different tissues, however, the combination of two or more parameters can enhance the segmentation. First, third and fourth pc-score showed a limited separation between vital and non-vital tissue. We have shown that Principal Component Analysis can be used for raw signal-enhancement data as well as for the contrast-concentration curves. In the future this study will be expanded using more datasets and other analysis methods. A method for (automatically) segmenting vital and non-vital tumor tissue according to the different parametric maps will be developed.

5. ACKNOWLEDGEMENT

This work was funded by the Dutch Cancer Society – KWF (grant no. 2008-4037).

6. REFERENCES

[1] T.E. Yankeelov, and J.C. Gore, "Dynamic Contrast- Enhanced Magnetic Resonance Imaging in Oncology: Theory, Data Acquisition, Analysis, and Examples," Curr. Med. Imaging Rev., 3(2), 91-107, 2009.

[2] D.M. McGrath et.al., "Comparison of Model-Based Arterial Input Functions for Dynamic Contrast-Enhanced MRI in Tumor Bearing Rats," Magn. Reson. in Medicine, 61, 1173–1184, 2009.

[3] M.J. Bruwer, J.F. MacGregor, and M.D. Noseworthy, "Dynamic Contrast-Enhanced MRI Diagnostics in Oncology via PCA," J. Chemometrics, 22, 708-716, 2008.

[4] P.S. Tofts, et.al., "Estimating Kinetic Parameters from Dynamic Contrast-Enhanced T1-Weighted MRI of a Diffusable Tracer: Standardized Quantities and Symbols," J. Magn. Reson. Imaging, 10(3), 223-232, 1999.

[5] E. Eyal, et.al., "Principal Component Analysis in Breast DCE-MRI Adjusted with a Model Based Method," J. Magn. Reson. Imaging, 30(5), 989–998, 2009.

[6] E. Eyal, et.al., "Principal Component Analysis for Dynamic Contrast-Enhanced MRI in Human Prostate Cancer," Invest. Radiol., 45, 174–181, 2010.

[7] L. Alic, et.al., "Facilitating Tumor Functional Assessment by Spatially Relating 3D Tumor Histology and In vivo MRI: Image Registration Approach," PLoS ONE, 6(8), 2011.

[8] K.Bol, et.al., "Developing a tool for the validation of quantitative DCE-MRI,"Proceedings of SPIE 7965, 79651J, 2011.

[9] S.C. Deoni, B.K. Rutt, T.M. and Peters, "Rapid combined T1 and T2 mapping using gradient recalled acquisition in the steady state, " Magn. Reson. Med., 49(3), 515-526, 2003.

[10] S. Wold, "Principal Component Analysis," Chemometrics and Intelligent Laboratory Systems, 2, 37-52, 1987.